

## PLANET FORMATION IN AB AURIGAE: IMAGING OF THE INNER GASEOUS SPIRALS OBSERVED INSIDE THE DUST CAVITY

YA-WEN TANG<sup>1</sup>, STEPHANE GUILLOTEAU<sup>2</sup>, ANNE DUTREY<sup>2</sup>, TAKAYUKI MUTO<sup>3</sup>, BO-TING SHEN<sup>4</sup>, PIN-GAO GU<sup>1</sup>, SHU-ICHIRO INUTSUKA<sup>5</sup>, MUNETAKE MOMOSE<sup>6</sup>, VINCENT PIETU<sup>7</sup>, MISATO FUKAGAWA<sup>8</sup>, EDWIGE CHAPILLON<sup>7</sup>, PAUL T. P. HO<sup>1</sup>, EMMANUEL DI FOLCO<sup>2</sup>, STUARTT CORDER<sup>9</sup>, NAGAYOSHI OHASHI<sup>10</sup>, AND JUN HASHIMOTO<sup>11</sup>

<sup>1</sup>Academia Sinica, Institute of Astronomy and Astrophysics, Taipei, Taiwan

<sup>2</sup>Laboratoire d'astrophysique de Bordeaux, Univ. Bordeaux, CNRS, B18N, alle Geoffroy Saint-Hilaire, 33615 Pessac, France

<sup>3</sup>Department of Physics, National Taiwan University, Taiwan

<sup>4</sup>Division of Liberal Arts, Kogakuin University, 1-24-2 Nishi-Shinjuku, Shinjuku-ku, Tokyo 163-8677, Japan

<sup>5</sup>Department of Physics, Graduate School of Science, Nagoya University, Furo-cho, Chikusa-ku, Nagoya 464-8602, Japan

<sup>6</sup>College of Science, Ibaraki University, 2-1-1 Bunkyo, Mito, Ibaraki 310-8512, Japan

<sup>7</sup>IRAM, 300 rue de la Piscine, Domaine Universitaire, 38406 Saint-Martin-d'Hères, France

<sup>8</sup>Division of Particle and Astrophysical Science, Graduate School of Science, Nagoya University, Furo-cho, Chikusa-ku, Nagoya, Aichi 464-8602, Japan

<sup>9</sup>National Radio Astronomy Observatory, 520 Edgemont Road, Charlottesville, VA, 22903, USA

<sup>10</sup>Subaru Telescope, National Astronomical Observatory of Japan, 650 North Aohoku Place, Hilo, HI 96720, USA and

<sup>11</sup>Astrobiology Center of NINS 2-21-1, Osawa, Mitaka, Tokyo, 181-8588, Japan

2017 Mar 9

### ABSTRACT

We report the results of ALMA observations of a protoplanetary disk surrounding the Herbig Ae star AB Aurigae. We obtained high-resolution ( $0''.1$ ; 14 au) images in  $^{12}\text{CO}$  ( $J=2-1$ ) emission and in dust continuum at the wavelength of 1.3 mm. The continuum emission is detected at the center and at the ring with a radius of  $\sim 120$  au. The CO emission is dominated by two prominent spirals within the dust ring. These spirals are trailing and appear to be about 4 times brighter than their surrounding medium. Their kinematics is consistent with Keplerian rotation at an inclination of  $23^\circ$ . The apparent two-arm-spiral pattern is best explained by tidal disturbances created by an unseen companion located at 60–80 au, with dust confined in the pressure bumps created outside this companion orbit. An additional companion at  $r$  of 30 au, coinciding with the peak CO brightness and a large pitch angle of the spiral, would help to explain the overall emptiness of the cavity. Alternative mechanisms to excite the spirals are discussed. The origin of the large pitch angle detected here remain puzzling.

*Subject headings:* protoplanetary disks — stars: individual (AB Aurigae) — planet-disk interactions

### 1. INTRODUCTION

Recent large facilities such as ALMA, Hi-CIAO/SUBARU or SPHERE/VLT have revealed complex gas and dust structures, such as large cavities, asymmetries and spiral patterns in protoplanetary disks, thanks to their high sensitivity and resolving power. The spiral-like features, either observed in the millimeter (mm) and sub-mm wavelengths or in the optical and infrared (IR) scattered light, are found around, for example, HD163296 (Grady et al. 2000; Fukagawa et al. 2010), HD100546 (Grady et al. 2001; Quanz et al. 2011), HD142527 (Fukagawa et al. 2006; Christiaens et al. 2014), HD97048 (Doering et al. 2007), MWC758 (Isella et al. 2010; Grady et al. 2013; Benisty et al. 2015), HD135344B (Muto et al. 2012), Elias 2-27 (Pérez et al. 2016), and HD141569A (Clampin et al. 2003; Perrot et al. 2016).

These spirals may appear reasonably regular, asymmetric or more reminiscent of faint discontinuous disks. The origin is basically due to gravitational disturbances, either via planet-disk interactions (e.g. Zhu et al. 2015) or gravitational instabilities inside a massive disk (Kratte & Lodato 2016). The resulting structures can be very complex (Dipierro et al. 2014; Dong et al. 2015; Flock et al. 2015; Pohl et al. 2015). Nevertheless, spiral-like

features are expected to reveal disturbers, such as embedded planets, which cannot be yet directly observed when the gas of the disk is not fully dissipated.

Located at 140 pc, AB Aurigae (hereafter AB Aur) is one of the closest Herbig Ae stars of spectral type of A0 Ve ( $2.4 \pm 0.2 M_\odot$ , DeWarf et al. 2003) and it shows an extended reflexion nebula at large scale (100s au). This young star is unique, because it exhibits a very small inner disk ( $\sim 2 - 5$  au) observed in near-IR (NIR) and mid-IR interferometry (di Folco et al. 2009), surrounded by a large cavity of radius  $\sim 70$  au based on the CO and mm continuum observations (Piétu et al. 2005), and a CO gas and dust rotating ring from which external spirals are observed both in the NIR (Fukagawa et al. 2004) and in the mm domain (Tang et al. 2012). The inclination of the inner and outer disks slightly varies from  $23^\circ$  at 20 au to  $29^\circ$  at 100 au scale (Tang et al. 2012). The accretion rate observed for AB Aur ( $1.3 \times 10^{-7} M_\odot \text{ yr}^{-1}$ ; Salyk et al. 2013; Garcia Lopez et al. 2006) is still high given the estimated age of the star (about 4 Myr).

The large scale spirals detected at optical/NIR wavelengths (Grady et al. 1999; Fukagawa et al. 2004) extend from 100 au up to 500 au. The extended CO emission mapped by the IRAM array also reveals large scale spirals. Tang et al. (2012) found that surprisingly, the excess of CO gas along the spirals is apparently counter-rotating with respect to the gaseous disk, that Tang et al.

(2012) attribute to residual gas being accreted from the envelope high above the disk mid-plane. Such a scenario is also reminiscent of the asymmetric accretion suggested for some Class 0 sources by Tobin et al. (2011).

At small scales, the wide dust gap, the warped disk (change in inclination from small to large scales by about 6-10 degrees) and the asymmetric dust ring (an intensity contrast of 3 is observed inside the mm dust ring), suggest the existence of, at least, one undetected companion with a mass of  $0.03 M_{\odot}$  at a radius of 45 au (Tang et al. 2012).

Motivated by such complex structures, we obtained ALMA observing time in Cycle 3 to image at very high angular resolution ( $< 0.1''$ ) the close environment of AB Aur in CO and in mm continuum. In this paper, we report the observations (Section 2) and the results (Section 3) of these data and then discuss them with respect to recent studies and models of planet-disk interactions (Section 4). For simpler comparison with previous work, we assume a distance of 140 pc, although GAIA DR1 release indicates  $153 \pm 10$  pc (Gaia Collaboration et al. 2016).

## 2. OBSERVATIONS

The observations were carried out with ALMA in Cycle 3 (project "2015.1.00889.S") with two execution blocks on Nov. 5 and Nov. 10, 2015, respectively. The array included 45 and 46 of the 12-m antennas, respectively. The baselines ranged from 78.1 m to 15.5 km. The gain calibrator (phase) is J0512+2927, which is 3.83 degree away from AB Aur and was observed with a cycle time between AB Aur and J0512+2927 of 1 minute. The band-pass calibrator was J0510+1800. The absolute flux level is referenced to J0423-0120 and J0510+1800 for which flux densities of 0.77 Jy and 3.42 Jy, respectively, were determined by the ALMA monitoring program. The flux calibration is expected to be accurate at the 10% level.

The calibrations were done by EA ARC using CASA 4.5. A secondary calibrator, J0518+3306, was observed every 15 minutes in order to verify the position accuracy. It lies 5.38 degree Eastwards of AB Aur, and is 3.83 degree away from the phase calibrator J0512+2927. After standard calibration, the position difference between the known coordinate and the apparent position of the secondary calibrator is  $0''.019$  and  $0''.036$  for the two execution blocks. We conclude that the absolute positioning accuracy of this experiment is limited to  $\sim 0''.03$ .

After calibration, the data were exported to the GILDAS package for further analysis. The detected central continuum peak of AB Aur at 1.3 mm is offset by  $(-5 \pm 0.3, -10 \pm 0.4)$  mas from the stellar location, taken from the Hipparcos reduction of van Leeuwen (2007). As this offset is of the same order as seen for the secondary calibrator, it is likely due to the absolute position uncertainties. We assume the continuum peak and the stellar positions are identical.

The presented data have been corrected for the proper motion with value of  $(2.63, -24.73)$  mas yr $^{-1}$  given by van Leeuwen (2007), and shifted to the epoch of 2000.0 for comparison with earlier work. All the presented maps are centered on the 1.3 mm continuum peak, which is at  $(\alpha, \delta) = (04:55:45.85, 30:33:04.30)$ . The maps of  $^{12}\text{CO}$  2-1 are with spectral resolution of  $0.71 \text{ km s}^{-1}$  and sensitivity of  $1.60 \text{ mJy per } 0''.11 \times 0''.08 \text{ beam}$  (4.6 K). The effective

sensitivity ( $1\sigma$ , including dynamic range limitations) of the continuum emission is  $33 \mu\text{Jy per } 0''.14 \text{ beam}$  (0.04 K).

## 3. RESULTS

### 3.1. Continuum Emission

The continuum emission at 1.3 mm is detected at  $60\sigma$  level toward the center, and clearly detected at the dust ring (Fig. 1b). The total detected flux density is 16.4 mJy, which is 20% of the reported flux density of 80 mJy at 1.3 mm from our previous detection with shorter baselines (Tang et al. 2012). This suggests that the missing 80% of the flux is at the scale larger than  $2''.1$ , which is determined by the shortest baseline of our observation. This missing flux at a scale larger than  $2''.1$  corresponds to a maximum brightness of the dust ring of  $\sim 0.2 \text{ mJy per } 0''.14 \text{ beam}$ . Accounting for this missing flux, the contrast in the dust ring between the brightest regions in the South-Eastern part and the rest can be as low as about 3, although Fig. 1a displays an apparent contrast around 5. The dust ring is consistent with a circular structure of radius  $\sim 120 \text{ au}$ , inclined at  $\sim 23^\circ$  with the same axis as derived from the gas kinematics by Piétu et al. (2005), and centered on the star. More precise values of the ring parameters are actually derived from higher sensitivity, lower angular resolution observations at 0.9 mm (Tang et al., in prep).

We model the central continuum peak with an elliptical disk in the visibility plane. The best fit disk diameter is found to be  $\sim 11 \text{ au}$ . The flux density is 2.1 mJy, which is larger than the previous detected value of 1.3 mJy with the IRAM interferometer (Tang et al. 2012). The difference is at  $3\sigma$  level when accounting for the flux calibration accuracy. Furthermore, the different spatial filtering properties of the two observations may also contribute to the measured differences, especially since the IRAM observations did not clearly separate the central continuum from the dust ring emission. We note that the total central continuum emission is about 3.4 mJy within the inner  $0''.6$  region and the emission appears extended at the level of SN ratio of 3.

The nature of the central continuum emission is unclear. There is an elongated emission at 3.3 cm detected with SN ratio of 4 along PA of  $\sim 170^\circ$  and was suggested as free-free jet by Rodríguez et al. (2014). The total flux density of the jet is reported to be 0.8 mJy at 7 mm. Assuming a spectral index of 0.6 for the jet, this free-free emission would give 2.2 mJy at 1.3 mm within the central  $1''$ . About 65% of the emission at 1.3 mm (2.1 mJy from the inner disk and 1.3 mJy from the faint emission) can come from free-free.

### 3.2. CO Gas

Previous observations of AB Aur in CO 2-1 and 3-2 at angular resolutions of  $\sim 0''.5 - 1''$  (Piétu et al. 2005; Lin et al. 2006) revealed that most of the gas was in a large outer disk surrounded by an extended envelope (Tang et al. 2012). The disk displayed an inner radius of 45 – 77 au (Piétu et al. 2005) depending on the isotopologue being observed, although some  $^{12}\text{CO}$  emission was associated with the unresolved inner dust disk (Tang et al. 2012). Large scale CO "spirals", extending outside the dust ring into the envelope, were reported in Lin

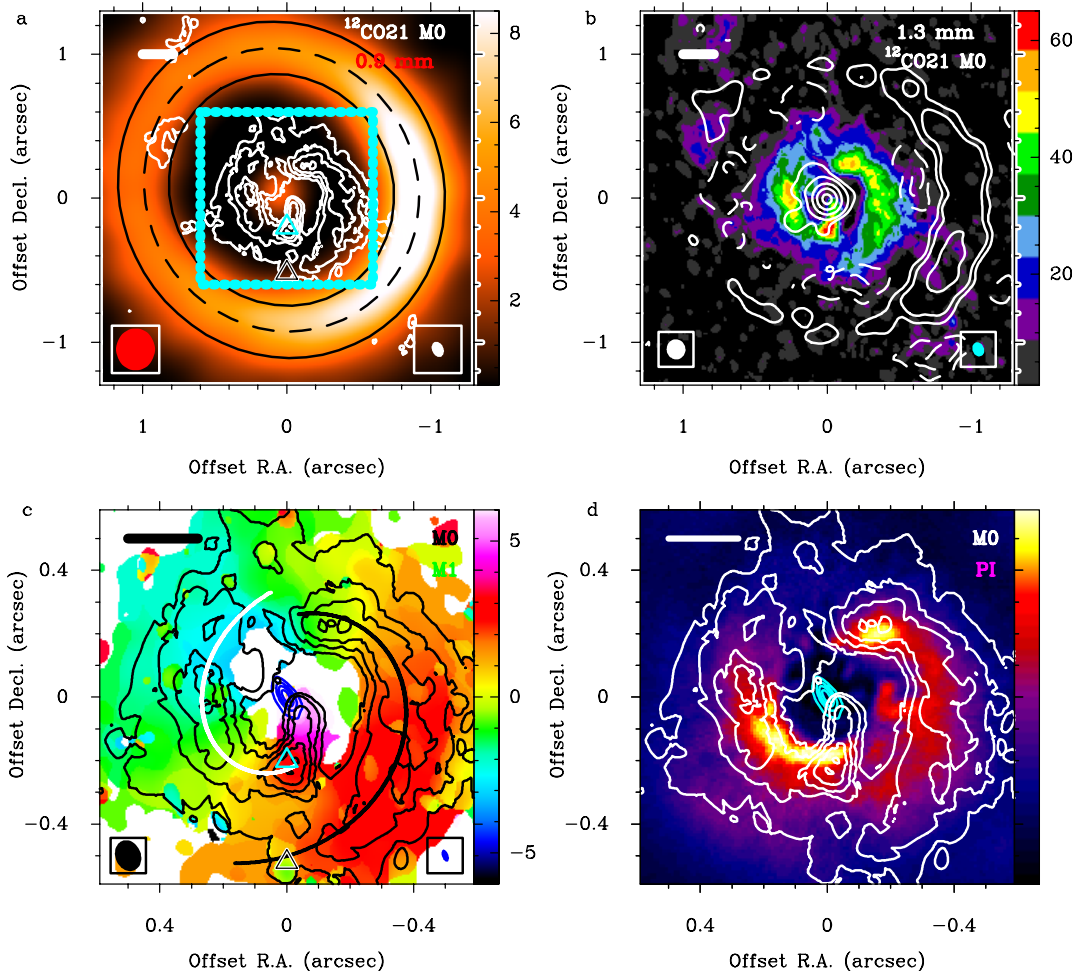


FIG. 1.— (a): Moment 0 map of CO 2-1 (contours) and 0.9 mm continuum (color scale; unit in mJy per  $0''.3$  beam; Tang et al., in prep). The cyan box marks the zoom-in area shown in panel c and d. The triangle marks the possible locations of the planets. (b): Continuum emission at 230 GHz (1.3 mm) (contours) and the moment 0 map of CO (color scale; unit in mJy/beam km/s, where the beam is  $0''.11$ ). The contours are  $-6, -3, 3, 15, 30$  and  $50\sigma$ , where  $1\sigma$  is  $33 \mu\text{Jy}$  per  $0''.14$  beam ( $0.04$  K). (c) Moment 0 (black contours) and moment 1 with  $v_{\text{sys}}$  subtracted (color scale; unit in km/s) maps of CO with an angular resolution of  $0''.11$ . Continuum emission at 1.3 mm with  $0''.03 \times 0''.07$  beam (marked in the lower right corner) is shown in thin blue contours at 10, 20, 30 and  $40\sigma$ , where  $1\sigma$  is  $27 \mu\text{Jy}/\text{beam}$ . The white and black arcs mark the best-fit spirals. (d) Moment 0 map of CO (white contours) and polarized intensity image at NIR (color scale, arbitrary unit; adopted from Hashimoto et al. 2011). The cyan contours are the same as in panel c. A scale bar of 30 au is marked at each upper-left corner. In panel a,c and d, the black contours are 2,4,6,8 and  $10 \times 6.15$  (mJy/beam km/s). The angular resolution of the color image and contour image is marked as an ellipse at the lower-left and lower-right corner, respectively, in panel a,b, and c.

et al. (2006) and Tang et al. (2012). Their kinematics suggest that these features trace gas infalling onto the ring from well above and below the disk mid-plane (Tang et al. 2012). On the other hand, a recent analysis of the NIR images, which uses the spectral-energy-distribution fitting, argue that these large scale spirals can be disk-related (Lomax et al. 2016). In any case, all structures reported in these earlier studies are at  $r > 100$  au and beyond.

In contrast, the new high angular resolution (about  $0''.1$ ) and high sensitivity (noise of 2.26 K)  $^{12}\text{CO}$  2-1 images obtained with ALMA (Fig. 1) reveal that most of the detected emission here is *inside* the dust cavity, within 90 au from the star. The  $^{12}\text{CO}$  2-1 emission at various velocity  $v_{\text{LSR}}$  (i.e. channel maps) is shown in Fig. 2. Fig.1 clearly shows that the CO gas is inside the dust ring and there is no apparent connection with the large CO disk and the extended CO spirals mentioned in the previous works. This apparent lack of connection

may, however, be partly an artefact due to our  $uv$  coverage. Any extended and smooth emission larger than about  $2''.1$  would have been filtered out. Only compact CO features, such as spirals or rings, remain detectable.

Some idea of the impact of this filtering can be obtained by comparing with the results from Tang et al. (2012), which included short spacings from a 30-m single dish map. Smoothing our data to the same angular resolution as in Tang et al 2012 ( $0''.56 \times 0''.42$ ) shows that we are only recovering 25 % of the line flux in the velocity ( $v_{\text{LSR}}$ ) range of 2 to 5 and 7 to 10 km/s. Near the systemic velocity ( $v_{\text{sys}}$  of 5.85 km/s) in  $v_{\text{LSR}}$  of 5 to 7 km/s, the missing flux problem is more severe. Given the typical brightness measured by Tang et al. (2012) of 50 K, we estimate that the measured brightness (at the velocity where the emission peaks) should be de-biased by adding about 20 to 30 K, as a first order correction for missing flux.

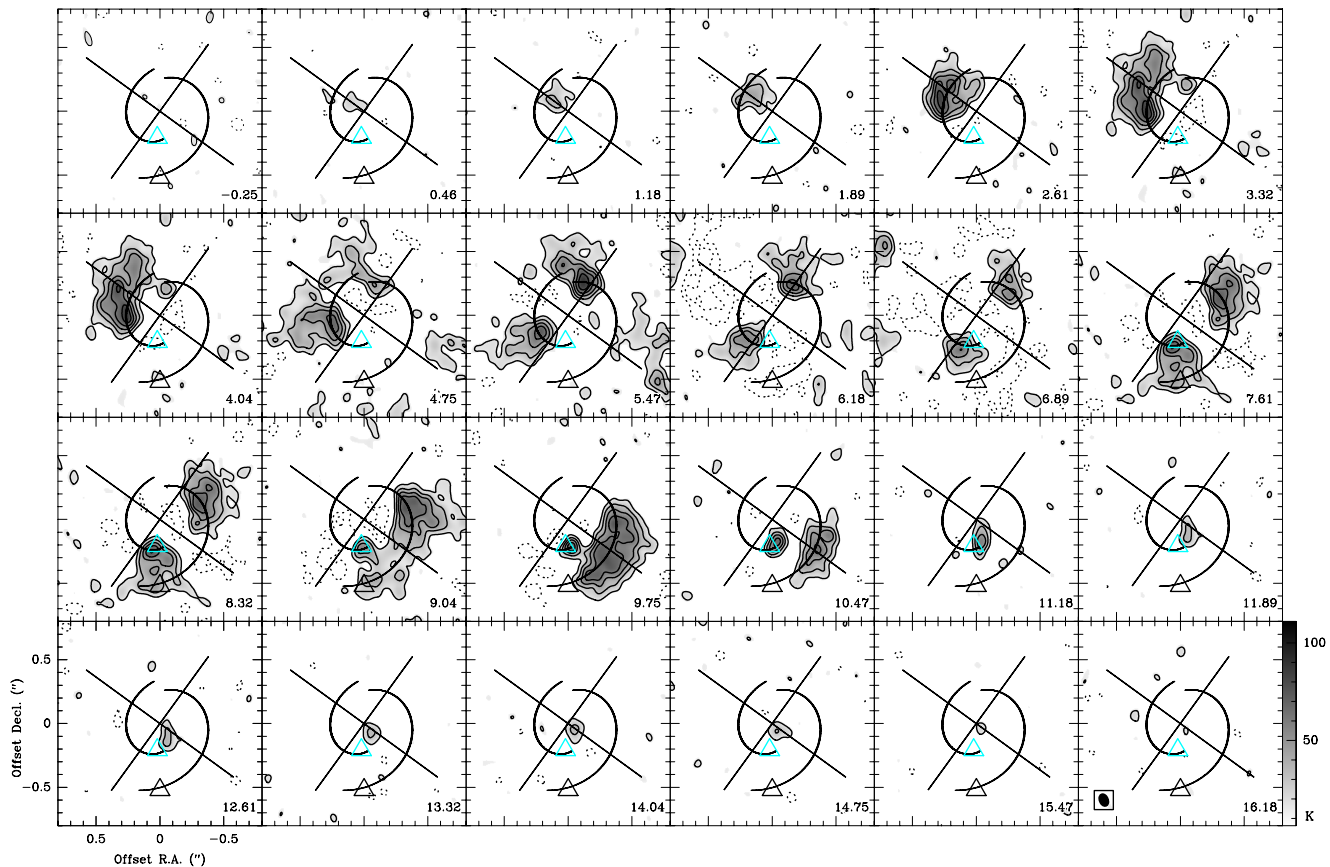


FIG. 2.— Channel maps of  $^{12}\text{CO}$  2-1. The contours denote the brightness temperature from -6,-3.3 to 15 by  $3\sigma$ , where  $1\sigma$  is 4.6 K (or 1.6 mJy per  $0''.11 \times 0''.08$  beam). The segments mark the major (P.A. of  $54^\circ$ ) and minor axis (P.A. of  $-36^\circ$ ) of the disk.  $v_{\text{LSR}}$  is labelled at the lower-right corner of each panel.

### 3.2.1. General Features

The detected  $^{12}\text{CO}$  2-1 gas emission peaks at position P1 (see Fig. 1), about 30 au from the star, where the peak brightness temperature,  $T_{\text{B}}$ , of 70 K at  $V_{\text{LSR}}$  of 8.32 km/s. At this distance, following Piétu et al. (2005), we assume CO traces gas at a temperature of 140 K. With a linewidth of  $1 \text{ km s}^{-1}$  and optically thin emission, the column density of CO gas is  $10^{17} \text{ cm}^{-2}$  (surface density,  $\Sigma_{\text{gas}}$ ,  $10^{-2} \text{ g/cm}^2$ ) for  $T_{\text{B}}$  of 70 K, which, for a CO gas abundance of  $10^{-4}$  with respect to  $\text{H}_2$ , gives a total gas mass of  $0.03 M_{\oplus}$  in one beam. As the CO gas emission is at least partially optically thick, this gas mass is only a lower limit. The non-detection of  $\text{C}^{18}\text{O}$  3-2 ( $3\sigma$  upper limit) indicates an upper limit for the mass 180 times larger (abundance ratio of CO to  $\text{C}^{18}\text{O}$  of 560), being  $5.4 M_{\oplus}$ .

The integrated intensity (moment 0) map of the  $^{12}\text{CO}$  2-1 emission appears asymmetric with respect to the central star (Fig. 1). The emission is patchy, especially in the fainter part, but appears to the first order spiral-like. We separate the CO emission into an eastern arm and a western arm for further analysis. The total gas mass of the eastern and western spirals is estimated to be in the order of  $1 M_{\oplus}$  or more.

To display the radius dependence of these structures, we present in Figure 3b the deprojected moment 0 map (see description below) in polar coordinates ( $r, \theta$ ), where  $r$  is the distance from the 1.3 mm continuum peak, and  $\theta$  is the Azimuth counted eastwards from North. Both

spirals appear to have a smaller  $r$  as azimuth increases, and are thus trailing given the known sense of rotation of the AB Aur disk. The eastern spiral consists of two separated structures, with the structures around azimuth of  $180^\circ$  having a clearer  $r$  dependence.

We further analyze the CO emission as follows. Firstly, the moment 0 map is deprojected with an inclination of  $23.2^\circ$  assuming the P.A. of the disk rotation axis of  $-36^\circ$  and centered on the 1.3 mm continuum peak (Fig. 3a). We then take the maximum locations of the  $^{12}\text{CO}$  moment 0 image every  $5^\circ$  in azimuth angle,  $\theta$ . We first fit the eastern and western arm with logarithmic spirals in order to search for the best description. For the eastern spiral, the best-fit function is  $r(\theta) = 0''.85 \exp(-21.0\theta)$ , where  $\theta$  is in degree, and the origin is at  $(-0''.01, -0''.09)$  from the continuum peak. Note that the data at  $r < 30$  au in the eastern spiral is clearly deviating from the best-fit function. In all the figures the best-fit function of the eastern spiral is not shown at  $r < 30$  au. For the western spiral, the best fit function is  $r(\theta) = 0''.38 \exp(-12.5\theta)$  and origin is at the central continuum peak. The results are marked in Fig. 3.

### 3.2.2. Kinematics

The highest velocities at which CO gas is detected are  $v_{\text{LSR}}$  of 0.46 and 15.47 km/s for the blue-shifted and red-shifted gas (see Fig. 1a), respectively. We note that the position centroid of the emission at these high velocities is consistent (within the uncertainty) with the location of the central continuum peak detected at 1.3 mm. Because

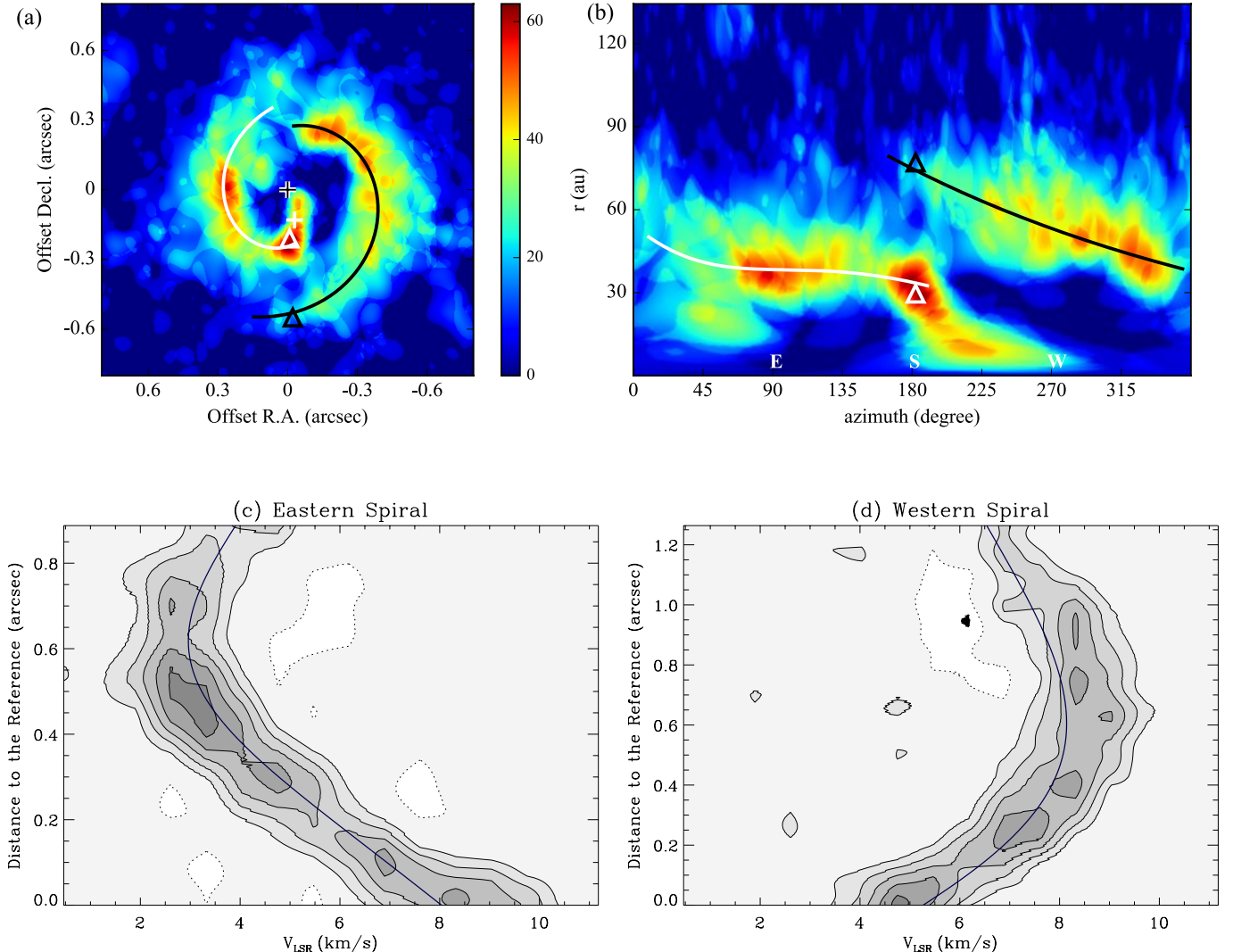


FIG. 3.— (a): De-projected moment 0 map of  $^{12}\text{CO}$  2-1 emission (in mJy/beam km/s). The arcs and pluses mark the best fit spiral and the origins of the best-fit in corresponding colors. The triangles mark the possible locations of the planets. (b): De-projected moment 0 map of  $^{12}\text{CO}$  in polar coordinate. The rest of the symbols are the same as in panel a. (c) and (d): Position-velocity plots of  $^{12}\text{CO}$  2-1 along the eastern and western spirals marked in panel a. The x-axis is  $v_{\text{LSR}}$  in units of km/s, and the y-axis is the distance to the starting point of the arm, which is the near end toward the star of the arm, in units of arcsecond. The contours are -3, 3, 6, 9, 12 and  $15\sigma$ , where  $1\sigma$  is 0.16 mJy per  $0''.11$  beam. The curves mark the expected Keplerian velocity with stellar mass of  $2.4 M_{\odot}$  and an inclination angle of  $23.2^{\circ}$  (solid line)

the peak locations of the high velocity CO gas appear along the disk plane, this suggests that the high velocity gas traces the inner CO disk in rotation instead of the jet observed at cm wavelengths by Rodríguez et al. (2014).

We extracted the position-velocity plots along the best-fit spirals (Figs. 3c and 3d). The predicted velocity due to Keplerian rotation ( $v_{\text{kep}}$ ) is indicated in solid line for the nominal inclination of  $23.2^{\circ}$  derived from the dust, a stellar mass,  $M_{\star}$ , of  $2.4 M_{\odot}$  and P.A. of the rotation axis of  $-36^{\circ}$ , using the systemic velocity,  $v_{\text{sys}}$ , of  $5.85 \text{ km s}^{-1}$  from Tang et al. (2012). There is no radial motion detected within the resolution of the reported observations ( $0''.1$  angular resolution and  $0.7 \text{ km/s}$  spectral resolution).

### 3.3. Comparison of ALMA observations with the optical/NIR images

Within the mm dust cavity, small dust grains ( $\mu\text{m}$  size) have been detected in scattered light in the optical and NIR (Grady et al. 1999; Fukagawa et al. 2004). The polarized intensity (PI) image at  $1.6 \mu\text{m}$  by Hashimoto et al. (2011) exhibits asymmetric features as a function of azimuth. The observed scattered light emission traces warm small dust particles at the top of the disk surface. Hashimoto et al. (2011) fitted two inclined rings and one ring gap to the PI emission. However, the derived orientations of the rings and the gap deviate from each other, suggesting that the actual structures are not rings. The CO gas distribution from our new results shows structures which are similar to those seen in the PI image (see Fig. 1d). Both trace the same spirals, but the  $1.6 \mu\text{m}$  features are inwards of the CO structures. We note that the small  $\mu\text{m}$  dust particles responsible for the  $1.6 \mu\text{m}$  scattering should be well mixed with the gas, as ob-

served in the case of IRS 48 by van der Marel et al. (2013). In addition, the extended CO emission is filtered out by ALMA.

#### 4. DISCUSSIONS

Several mechanisms can lead to spiral-like patterns. However, the AB Aur disk density is not large enough to make it gravitationally unstable at all scales (Piétu et al. 2005). The observation of spirals within the dust cavity rather points towards tidal disturbances by a compact object. We investigate here to what extent an embedded (planetary mass) object can explain the observed structures. Such an object located inside the dust cavity may create both the observed mm cavity and spiral-like pattern (for example, Zhu et al. 2015).

In Dong et al. (2015), the adiabatic model with a  $6 M_J$  planet orbiting at 50 au of  $M_\star = 1 M_\odot$  seems to produce structures similar to what we observe here in  $^{12}\text{CO}$ . Scaling to the mass of AB Aur ( $M_\star$  of  $2.4 M_\odot$ ), the planet would need to have a mass of  $14 M_J$  and be located at  $r$  of 30 au (location P1, see section 3.2.1; figure 1c), in order to create the observed features if we adopt this model.

This possibility is supported by several unusual features detected near the location of this putative inner planet at P1. First, the pitch angle of the eastern spiral becomes large near this point: large pitch angles are only obtained near the driving object in planetary-induced spirals. Second, there is a compact CO emission between at velocities  $v_{\text{LSR}}$  of 9.04 to 11.18 km/s (see Fig. 2) and the linewidth is larger than elsewhere, as expected for the streaming motions (gas accretion and jet at the circumplanetary disk) around the planet (see Gressel et al. 2013, , for example). Finally, there is 1.3 mm continuum emission with flux of  $110 \mu\text{Jy}/\text{beam}$  at the location P1. This matches the predicted flux densities of the circumplanetary disks of known planet candidates, of the order of  $100 \mu\text{Jy}$  at 1.3 mm (Zhu et al. 2016). However, because the 3.3 cm continuum flux is  $35.9 \mu\text{Jy}/\text{beam}$  at this position, we can not rule out that the 1.3 mm continuum emission has a contribution from free-free emission.

However, this scenario faces some difficulties. In the analysis of the multi-epoch NIR images, Lomax et al. (2016) found no apparent rotation of the spiral patterns within the 5.8 year time span of the images. If the spiral patterns are induced by a planet or companion, this suggests that such an object is located at  $r > 47$  au. However, their first epoch data, using Stokes I only, is not sensitive to the region around P1 discussed here, so this result only applies to the other arms. Furthermore, a planet at P1 cannot simply explain the western spiral, because outwards of the orbit of the driving planet, the perturbation is mostly a (usually tightly wound) one arm spiral.

On the contrary, two-arm spirals are easily produced inside the orbit of the perturbing planet (see Fung & Dong 2015, , for example). In this second scenario, another possible location of the planet, P2, is at the outertip of the western spiral (i.e. at P.A. of  $180^\circ$  and  $r = 80$  au). In this case, the spirals seen here are inner spirals, and the two arms are explained by a single perturber. A planet at this location can also explain the sharp inner edge of the dust ring seen at 1.3 mm, while there is still a significant amount of  $\mu\text{m}$  size dust particles (Hashimoto

et al. 2011) within the mm dust cavity. This is consistent with the picture of dust filtration, where dust grains larger than 0.1 mm are trapped at the radius outside of the planet and only small dust grains and gas can accrete toward the inner disk (Zhu et al. 2012). This location is also far enough to be consistent with the lack of apparent rotation of the NIR spiral patterns found by Lomax et al. (2016).

The main difficulty in this scenario is its failure to explain the large pitch angle between P1 and the star location. One possibility would be that the inner disk part of the system is warped compared to the outer part. Indeed, attributing a single inclination to the AB Aur system appears challenging. The inclination angle of the dust ring is  $23^\circ$ , while NIR interferometric results suggest an inclination of only  $20^\circ$  for the inner dust disk (Eisner et al. 2004). The larger scale observations from Piétu et al. (2005) suggest higher inclinations, but fail to reproduce the expected Keplerian velocities. It appears that the variation of inclination as a function of scale can not explain the large pitch angle.

All the spirals induced by planets in simulations appear to have limited contrast, the maximum being 2:1 in Dong et al. (2015), for example. The  $^{12}\text{CO}$  spiral is detected at about  $12\sigma$  level (see figure 3c and 3d). Using a  $3\sigma$  non-detection of the surroundings, the observed spirals have a contrast of 4:1, much higher than predictions. However, the missing flux (see section 3.2) can easily bring down this contrast to 2:1. Furthermore, the models predict density contrasts, while we observe a brightness contrast in the CO J=2-1 line.

The simplest interpretation of the observed contrast is linked to the vertical thermal gradient in the disk and the expected CO opacity. The spirals have larger column densities, and the  $\tau = 1$  layer is reached at higher heights in the spirals. Therefore, the spirals are warmer gas and far from being dense enough to affect the local scale height. We note that from a comparison between  $^{12}\text{CO}$  and  $^{13}\text{CO}$ , Piétu et al. (2005) indicated a temperature difference of about a factor of 2 between the lower layer traced by  $^{13}\text{CO}$  and the  $^{12}\text{CO}$  surface. Beside, the near-IR opacity towards the star is much larger than the CO line opacity along our line of sight. We expect the scattered light to trace the inner side of the spiral structures, exactly as seen in Fig. 1d.

These spiral-like patterns are reminiscent of the patterns expected for planet-induced structures in disks, although the pitch angle seems relatively large (about  $20^\circ$  for the Western spiral). Indeed, it is difficult to fit the analytical shape prescription of Rafikov (2002); Muto et al. (2012) to our measurement. For the south part of the Eastern spiral, we find a planet location near 28 au at PA  $180^\circ$  (i.e. near the brightest spot) but the best fit values for parameters  $h/r$  at the planet radius and  $\beta$  (the exponent of the velocity law of the sound speed) are 0.4 and 0.9, respectively. This is inconsistent with the measured radial temperature profile and expected thickness of our disk, as derived from hydrostatic equilibrium. The Western spiral analysis lead to similar difficulties, although a solution with a planet near 20 au is possible assuming  $\beta = 0$ .

Another exciting mechanism of the spiral wave is suggested by Montesinos et al. (2016), where shadows cast by a tilted inner disk onto the outer disk will cause a drop

in illumination and thus lower temperature locally. The pressure imbalance will further cause a density enhancement. As suggested, this mechanism could create spiral waves with an opening angle  $10\text{--}15^\circ$  in the outer disk. We note that the CO spirals detected here are within the cavity. Furthermore, there is no evidence for strong tilt of the inner (few au) disk of AB Aur compared to the observed spirals, so this mechanism is unlikely to apply to our case.

Spiral patterns can also develop under external disturbances, like asymmetric accretion (Hennebelle et al. 2016b,a). Again, these studies assume a centrally condensed disk, different from the spirals detected here within the dust ring. Indeed, for AB Aur, accretion from the outer envelope was invoked by Tang et al. (2012) to explain the apparent counter-rotation of the gas in the outer (150–400 au) spirals. However, the opening angle of the induced spiral pattern is expected to be on the order of  $h/r$  in the Hennebelle et al. (2016b) model, again much smaller than our 0.3 radian value.

Thus, while our trailing spirals are highly suggestive of disturbances due to planet-disk interaction or external disturbances, their pitch angle seems difficult to explain. We point out, however, that this apparent opening angle is only defined through a relatively limited range of azimuth (less than  $180^\circ$ ). Furthermore, it may be affected by differential filtering of the extended emission

at the various velocities (see section 3.2), especially near  $v_{\text{sys}}$  where the missing flux is largest. The effect of missing flux on the morphology of the detected spirals can be studied by combining new ALMA observations with shorter baselines covering the size-scale of the spirals.

In summary, we report the detection of gaseous spirals within dust gap for the first time in the transitional disk AB Aur. In contrast to previous detections of the spirals in continuum emission, we are able to probe the kinematics of the spirals, which is mainly Keplerian. We argue that the spirals are most likely triggered by embedded object at two possible locations, either at 60–80 au and/or at around 30 au from the star.

*Facilities:* ALMA.

This paper makes use of the following ALMA data: ADS/JAO.ALMA#2015.1.00889.S. ALMA is a partnership of ESO (representing its member states), NSF (USA) and NINS (Japan), together with NRC (Canada), NSC and ASIAA (Taiwan), and KASI (Republic of Korea), in cooperation with the Republic of Chile. The Joint ALMA Observatory is operated by ESO, AUI/NRAO and NAOJ. This research was partially supported by MOST grant MOST 105-2112-M-001-025-MY3. This research was supported in part by the "Programme National de Physique Stellaire" from INSU/CNRS, France.

#### REFERENCES

- Benisty, M., et al. 2015, *A&A*, 578, L6  
 Christiaens, V., Casassus, S., Perez, S., van der Plas, G., & Ménard, F. 2014, *ApJ*, 785, L12  
 Clampin, M., et al. 2003, *AJ*, 126, 385  
 DeWarf, L. E., Sepinsky, J. F., Guinan, E. F., Ribas, I., & Nadalin, I. 2003, *ApJ*, 590, 357  
 di Folco, E., Dutrey, A., Chesneau, O., Wolf, S., Schegerer, A., Leinert, C., & Lopez, B. 2009, *A&A*, 500, 1065  
 Dipierro, G., Lodato, G., Testi, L., & de Gregorio Monsalvo, I. 2014, *MNRAS*, 444, 1919  
 Doering, R. L., Meixner, M., Holfeltz, S. T., Krist, J. E., Ardila, D. R., Kamp, I., Clampin, M. C., & Lubow, S. H. 2007, *AJ*, 133, 2122  
 Dong, R., Zhu, Z., Rafikov, R. R., & Stone, J. M. 2015, *ApJ*, 809, L5  
 Eisner, J. A., Lane, B. F., Hillenbrand, L. A., Akeson, R. L., & Sargent, A. I. 2004, *ApJ*, 613, 1049  
 Flock, M., Ruge, J. P., Dzyurkevich, N., Henning, T., Klahr, H., & Wolf, S. 2015, *A&A*, 574, A68  
 Fukagawa, M., Tamura, M., Itoh, Y., Kudo, T., Imaeda, Y., Oasa, Y., Hayashi, S. S., & Hayashi, M. 2006, *ApJ*, 636, L153  
 Fukagawa, M., et al. 2004, *ApJ*, 605, L53  
 —. 2010, *PASJ*, 62, 347  
 Fung, J., & Dong, R. 2015, *ApJ*, 815, L21  
 Gaia Collaboration, Brown, A. G. A., Vallenari, A., Prusti, T., de Bruijne, J., Mignard, F., Drimmel, R., & co-authors, . 2016, *ArXiv e-prints*  
 Garcia Lopez, R., Natta, A., Testi, L., & Habart, E. 2006, *A&A*, 459, 837  
 Grady, C. A., Woodgate, B., Bruhweiler, F. C., Boggess, A., Plait, P., Lindler, D. J., Clampin, M., & Kalas, P. 1999, *ApJ*, 523, L151  
 Grady, C. A., et al. 2000, *ApJ*, 544, 895  
 —. 2001, *AJ*, 122, 3396  
 —. 2013, *ApJ*, 762, 48  
 Gressel, O., Nelson, R. P., Turner, N. J., & Ziegler, U. 2013, *ApJ*, 779, 59  
 Hashimoto, J., et al. 2011, *ApJ*, 729, L17+  
 Hennebelle, P., Lesur, G., & Fromang, S. 2016a, *ArXiv e-prints*  
 —. 2016b, *A&A*, 590, A22  
 Isella, A., Carpenter, J. M., & Sargent, A. I. 2010, *ApJ*, 714, 1746  
 Kratter, K., & Lodato, G. 2016, *ARA&A*, 54, 271  
 Lin, S.-Y., Ohashi, N., Lim, J., Ho, P. T. P., Fukagawa, M., & Tamura, M. 2006, *ApJ*, 645, 1297  
 Lomax, J. R., et al. 2016, *ArXiv e-prints*  
 Montesinos, M., Perez, S., Casassus, S., Marino, S., Cuadra, J., & Christiaens, V. 2016, *ApJ*, 823, L8  
 Muto, T., et al. 2012, *ApJ*, 748, L22  
 Pérez, L. M., et al. 2016, *Science*, 353, 1519  
 Perrot, C., et al. 2016, *A&A*, 590, L7  
 Piétu, V., Guilloteau, S., & Dutrey, A. 2005, *A&A*, 443, 945  
 Pohl, A., Pinilla, P., Benisty, M., Ataiee, S., Juhász, A., Dullemond, C. P., Van Boekel, R., & Henning, T. 2015, *MNRAS*, 453, 1768  
 Quanz, S. P., Schmid, H. M., Geissler, K., Meyer, M. R., Henning, T., Brandner, W., & Wolf, S. 2011, *ApJ*, 738, 23  
 Rafikov, R. R. 2002, *ApJ*, 569, 997  
 Rodríguez, L. F., Zapata, L. A., Dzib, S. A., Ortiz-León, G. N., Loinard, L., Macías, E., & Anglada, G. 2014, *ApJ*, 793, L21  
 Salyk, C., Herczeg, G. J., Brown, J. M., Blake, G. A., Pontoppidan, K. M., & van Dishoeck, E. F. 2013, *ApJ*, 769, 21  
 Tang, Y.-W., Guilloteau, S., Piétu, V., Dutrey, A., Ohashi, N., & Ho, P. T. P. 2012, *A&A*, 547, A84  
 Tobin, J. J., et al. 2011, *ApJ*, 740, 45  
 van der Marel, N., et al. 2013, *Science*, 340, 1199  
 van Leeuwen, F. 2007, *A&A*, 474, 653  
 Zhu, Z., Dong, R., Stone, J. M., & Rafikov, R. R. 2015, *ApJ*, 813, 88  
 Zhu, Z., Ju, W., & Stone, J. M. 2016, *ArXiv e-prints*  
 Zhu, Z., Nelson, R. P., Dong, R., Espaillat, C., & Hartmann, L. 2012, *ApJ*, 755, 6